Ab initio calculations of the structure and mechanical properties of vanadium oxides

2009 J. Phys.: Condens. Matter 21 145404

(http://iopscience.iop.org/0953-8984/21/14/145404)

J. Phys.: Condens. Matter **21** (2009) 145404 (8pp) doi:10.1088/0953-8984/21/14/145404

Ab initio calculations of the structure and mechanical properties of vanadium oxides

Thomas Reeswinkel, Denis Music and Jochen M Schneider

Materials Chemistry, RWTH Aachen University, D-52056 Aachen, Germany

E-mail: reeswinkel@mch.rwth-aachen.de

Received 30 October 2008, in final form 13 February 2009
Published 9 March 2009
Online at stacks.iop.org/JPhysCM/21/145404

Abstract

VO, V_2O_3, VO_2, V_6O_{13}, V_4O_9, V_3O_7 and V_2O_5 have been investigated in terms of structure, bulk modulus B and elastic constant C_{44} using *ab initio* calculations. The C_{44} values for V_6O_{13}, V_4O_9, V_3O_7 and V_2O_5 are significantly lower than those for V_2O_3 and VO_2. As the V valency is increased from 3 to 5, C_{44} decreases by 83%, whereas the bulk modulus decreases by 61%, leading to an increase in the B/C_{44} ratio from 1.4 to 3.4. This is consistent with calculated decohesion energies for cleavage in VO_2 and V_2O_5. When cleaving V_2O_5, decohesion energies are considerably lower than those of VO_2. This behaviour may be understood based on V valency induced changes in the crystal and electronic structure as well as in the chemical bonding. As the V valency is increased, the bond strength decreases. The phases with a V valency >4 exhibit low C_{44} values, large anisotropy and possess weak ionic bonding between the layers. The formation of easily plastically deformable structures is enabled by the screened Coulomb potential. The largest distance and therefore weakest bond strength is observed for V_2O_5 in the (002) plane.

(Some figures in this article are in colour only in the electronic version)

1. Introduction

Vanadium oxides are of great interest in multiple applications, mainly because of the wide range of valency that is exhibited by V, which affects the physical and chemical properties of the oxides. Homologous series within the vanadium oxide phase diagram have been constructed [1–4], often referred to as Magnéli series, such as the V_nO_{2n-1} series between the borderline phases V_2O_3 ($n = 2$) and VO_2 ($n = \infty$) [5] and the V_nO_{2n+1} series between the borderline phases VO_2 ($n = \infty$) and V_2O_5 ($n = 2$) [6]. A large range of vanadium oxides can be used as catalysts [7], e.g. for partial or selective oxidation reactions, also in conjunction with other transition metal oxides, such as titanium, molybdenum or tungsten oxides. Density functional theory calculations have been carried out, often within the scope of surface studies [8–12]. Several vanadium oxides exhibit a metal-to-insulator phase transition from a high temperature metallic phase to a low temperature insulating or semiconductive phase [13–18]. Here, the V_nO_{2n-1} series is of particular interest [4, 19–22], but also other phases are taken into account [23, 24]. Some vanadium bronzes, usually non-stoichiometric compounds incorporating (earth) alkali metals, feature interesting magnetic behaviour [25]. In addition, certain vanadium oxide phases have been reported as being promising materials for intermediate to high temperature metal cutting applications. It has been suggested that this is due to easily activated shear planes [26–28]. When annealing TiAlN/VN superlattice thin films, the friction coefficient is significantly reduced, due to the formation of V_nO_{2n+1} phases [29]. However, no systematic studies on the elastic properties of these vanadium oxides have been published.

The objective of this work is to contribute towards an understanding of the correlation between composition, structure and elastic properties of vanadium oxides. Our strategy is to apply *ab initio* calculations to obtain the bulk modulus and the elastic constant C_{44} (as a measure of the shear modulus) [30, 31] for seven different vanadium oxides VO_x ($1 \leqslant x \leqslant 2.5$) with vanadium valency from 2 to 5, including three mixed-valency phases, and correlate these with the electronic structure thereof. Namely, these phases are VO (rock salt structure) [32], V_2O_3 (karelianite, corundum structure) [33], VO_2 (rutile structure) [34], V_6O_{13} [35], V_4O_9 [36], V_3O_7 [37] and V_2O_5 (shcherbinaite) [38]. The latter five belong to the V_nO_{2n+1} homologous series between VO_2 ($n = \infty$) and V_2O_5 ($n = 2$). As the V valency is

increased from 3 to 5, crystal structure and chemical bonding changes are observed; C_{44} decreases by 83%, whereas the bulk modulus values decrease by 61%, leading to an increase in the B/C_{44} ratio from 1.4 to 3.4. This is consistent with calculated decohesion energies for cleavage in VO_2 and V_2O_5. When cleaving V_2O_5 in the (002) plane, decohesion energies are extremely low, as compared to VO_2. This behaviour may be understood based on V valency induced changes in electronic structure.

2. Methods

Calculations in this work were carried out using density functional theory (DFT) [39] as implemented in the *Vienna ab initio simulation package* (VASP), in which projector augmented wave potentials with the Perdew–Wang (PW91) generalized-gradient approximation are employed [40, 41] with so-called Blöchl corrections for the total energy [42]. The convergence criterion for the total energy was 0.01 meV within a 500 eV cutoff. Integration in the Brillouin zone was done on special k-points, according to Monkhorst–Pack [43]. All configurations were studied on a mesh of $7 \times 7 \times 7$ irreducible k-points (unless otherwise noted). Equilibrium values for the lattice parameters were obtained by fitting the total energy versus a, b/a or c/a, with third order polynomials. All structures were relaxed with respect to atomic positions and Wigner–Seitz primitive cell volume. Initial structural data for the *ab initio* calculations were taken from the literature for VO (rock salt structure) [32], V_2O_3 (karelianite, corundum structure) [33], VO_2 (rutile structure) [34], V_6O_{13} [35], V_4O_9 [36], V_3O_7 [37] and V_2O_5 (shcherbinaite) [38]. As a comparison, α-Al_2O_3 (corundum) [33] and TiO_2 (rutile) [34] as the structural prototypes for V_2O_3 and VO_2, respectively, were also calculated in the same way. These well-known structures can be used to verify the methodology applied in this work, since relevant experimental data are available.

To obtain information about the stability of the phases studied, the energy of formation per atom (E_f) with respect to the elements was calculated as the total energy difference between the compound phases probed and the said elements:

$$E_f(V_xO_y) = \frac{E(V_xO_y) - (x\,E(V) + \frac{1}{2}y\,E(O_2))}{x+y}.$$

Thereby, the total energies of bcc vanadium [44] and O_2 were calculated. To obtain the total energy of O_2, a cubic cell was created with one oxygen atom at the cell's origin and another one along the distance of the O=O π-bond length (120.741 pm) [45] in one lattice direction. The lattice parameter was set to 12 Å, anticipating negligible interactions between periodic images.

The bulk modulus B was obtained by fitting the energy–volume curves to the Birch–Murnaghan equation of states [46], with volume (de)compression of $\pm 5\%$ and $\pm 10\%$. The elastic constant C_{44} was determined according to the methods developed by Mehl *et al* for cubic [47] and tetragonal [48] phases, Ravindran *et al* [49] for orthorhombic phases and Fast *et al* [50] for hexagonal phases with shear stains of $\pm 1\%$ and $\pm 2\%$. C_{44} is proportional to the shear modulus and can be used as a measure of the shear resistance [30, 31]. Due to expectedly large structural anisotropy for some phases, calculations for obtaining B and C_{44} were carried out in two different ways, (i) considering uniform compression (full structural relaxation only at equilibrium and no further relaxations for determination of lattice parameters and elastic constants), and (ii) with full structural relaxations at every volume for determination of elastic constants. The latter procedure yielded more precise results in the case of anisotropic structures, such as hydroxyapatite [51], Nb_2S_2C [52], boron nitrides [53] and graphite [54].

Furthermore, electron density distributions (EDD) were evaluated to contribute towards the understanding of the correlation between the bonding and elastic properties. EDD data were analysed using VESTA [55]. The same settings were applied for each data set.

In order to study cleavage in VO_2 and V_2O_5, the decohesion energies for cleavage G were calculated as the energy required for the separation of the structure into two blocks [56, 57]. This energy depends on the cleavage distance between these two separated blocks until it reaches a constant level at a certain distance. No structural relaxation was allowed during the separation [56, 57]. Cleavages were considered in {100} and {200} planes in each (independent) lattice direction. To obtain the (200) cleavage, the cell was cut into two blocks: with one block ranging from fractional coordinate $0 \leqslant x < 0.5$ (of the original unit cell) and the other ranging from $0.5 \leqslant x < 1$. Calculations were carried out up to a cleavage distance of 10 Å, at which G remained constant. To avoid interaction between the cleaved planes due to periodic boundary conditions, supercells containing 16 atomic layers normal to the cleavage plane were constructed with a proportionate mesh of irreducible k-points. Therefore, in order to cleave VO_2 in x or symmetrical y direction and in z direction, $3 \times 1 \times 1$ and $1 \times 1 \times 8$ supercells and meshes of $1 \times 5 \times 5$ and $5 \times 5 \times 1$ irreducible k-points were constructed, respectively. To cleave V_2O_5 in x, y and z direction, $3 \times 1 \times 1$, $1 \times 8 \times 1$ and $1 \times 1 \times 8$ supercells and meshes of $1 \times 3 \times 3$, $3 \times 1 \times 3$ and $3 \times 3 \times 1$ irreducible k-points were constructed, respectively. Convergence tests with larger k-point meshes were performed and the difference was found to be negligible. For example, the difference in decohesion energy of the V_2O_5 $3 \times 1 \times 1$ supercell (100) between k-point meshes of $1 \times 3 \times 3$ and $5 \times 5 \times 5$ was less than 1%.

3. Results and discussion

The calculated structural data of the different phases—formula, space group, lattice parameters, volume (per atom) and number of formula units per unit cell (Z)—as well as fractional atomic coordinates and Wyckoff positions, are presented for VO (rock salt structure, $Fm\bar{3}m$) in table 1, V_2O_3 (karelianite structure, the vanadium counterpart of corundum, $R\bar{3}c$) in table 2, VO_2 (rutile structure, $P4_2/mnm$) in table 3, V_6O_{13} ($Cmma$) in table 4, V_4O_9 ($Pnma$) in table 5, V_3O_7 ($I4/mmm$) in table 6 and V_2O_5 (shcherbinaite, $Pmmn$) in table 7.

VO, table 1, exhibits rock salt structure with a calculated lattice parameter $a = 4.186$ Å for an ideal, stoichiometric

Table 1. VO cell description.

Formula		VO		
Space group		$Fm\bar{3}m(225)$		
a (Å)		4.186		
V (Å^3/atom)		9.169		
Z		4		
Atom	Site	x	y	z
V	4b	0	0	0
O	4a	0.5	0.5	0.5

Table 2. V_2O_3 cell description with hexagonal axes.

Formula		V_2O_3		
Space group		$R\bar{3}c(167)$ (Hexagonal axes)		
a (Å)		4.925		
c (Å)		13.834		
V (Å^3/atom)		9.687		
Z		6		
Atom	Site	x	y	z
V	12c	0	0	0.341
O	18e	0.329	0	0.25

Table 3. VO_2 cell description.

Formula		VO_2		
Space group		$P4_2/mnm(136)$		
a (Å)		4.558		
c (Å)		2.858		
V (Å^3/atom)		9.897		
Z		2		
Atom	Site	x	y	z
V	2a	0	0	0
O	4f	0.300	0.300	0

Table 4. V_6O_{13} cell description.

Formula		V_6O_{13}		
Space group		$Cmma(67)$		
a (Å)		11.935		
b (Å)		19.940		
c (Å)		3.687		
V (Å^3/atom)		11.545		
Z		4		
Atom	Site	x	y	z
V	16o	0.147	0.069	0.75
V	8n	0.148	0.25	0.75
O	16o	0.174	0.049	0.25
O	16o	0.151	0.153	0.75
O	8n	0.177	0.25	0.25
O	8m	0	0.056	0.75
O	4g	0	0.25	0.75

Table 5. V_4O_9 cell description.

Formula		V_4O_9		
Space group		$Pnma(62)$		
a (Å)		17.910		
b (Å)		3.642		
c (Å)		9.452		
V (Å^3/atom)		11.858		
Z		4		
Atom	Site	x	y	z
V	4c	0.491	0.25	0.274
V	4c	0.080	0.25	0.543
V	4c	0.163	0.25	0.205
V	4c	0.313	0.25	0.449
O	4c	0.024	0.25	0.727
O	4c	0.449	0.25	0.049
O	4c	0.339	0.25	0.654
O	4c	0.198	0.25	0.005
O	4c	0.088	0.25	0.341
O	4c	0.047	0.25	0.088
O	4c	0.392	0.25	0.357
O	4c	0.167	0.25	0.584
O	4c	0.240	0.25	0.316

Table 6. V_3O_7 cell description.

Formula		V_3O_7		
Space group		$I4/mmm(139)$		
a (Å)		13.986		
c (Å)		3.631		
V (Å^3/atom)		11.838		
Z		6		
Atom	Site	x	y	z
V	2a	0	0	0
V	8h	0.184	0.184	0
V	8i	0.366	0	0
O	2b	0	0	0.5
O	8h	0.099	0.099	0
O	8h	0.294	0.294	0
O	8j	0.094	0.5	0
O	16l	0.290	0.093	0

Table 7. V_2O_5 cell description.

Formula		V_2O_5		
Space group		$Pmmn(59)$		
a (Å)		11.532		
b (Å)		3.600		
c (Å)		4.401		
V (Å^3/atom)		13.051		
Z		2		
Atom	Site	x	y	z
V	4f	0.102	0.25	0.890
O	4f	0.106	0.25	0.523
O	4f	0.931	0.25	0.003
O	2a	0.25	0.25	0.004

crystal without defects. This is slightly larger than the experimental value of 4.12 Å [32], resulting in a volume difference of 4.9%. Since VO is defect stabilized and exhibits vacancy concentrations of approximately 15% for both metallic and oxygen sites [58], this deviation seems reasonable. All other vanadium oxides considered, i.e. V_2O_3 (table 2), VO_2

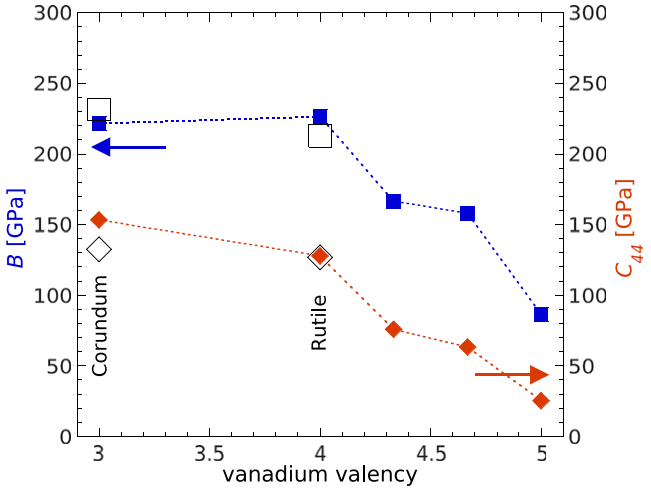

Figure 1. Bulk modulus B (squares/blue) and elastic constant C_{44} (diamonds/red) as a function of vanadium valency. Corundum and rutile are included for comparison and shown in open symbols.

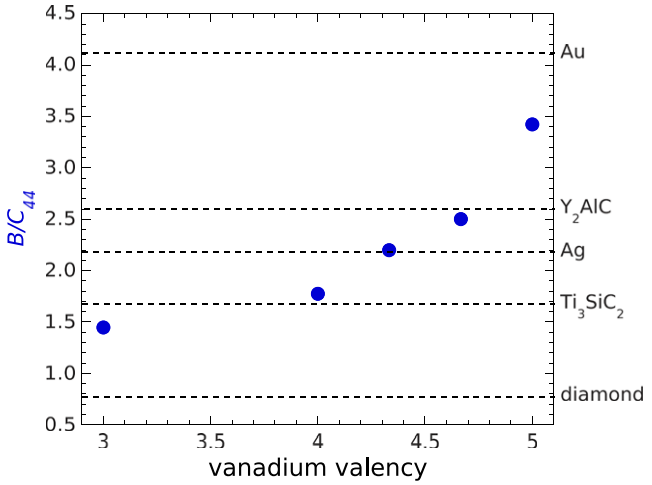

Figure 2. B/C_{44} ratio as a function of vanadium valency. Experimental values for diamond, silver and gold [64] as well as calculated values for MAX phase nanolaminates, Ti_3SiC_2 [65] and Y_2AlC [66], are shown as dashed lines for comparison.

(table 3), V_6O_{13} (table 4), V_4O_9 (table 5), V_3O_7 (table 6) and V_2O_5 (table 7), exhibit better agreement with previously published structural data [33–38]. The deviations between the calculated and measured lattice parameter values are within 0.1–1.2%, except for V_3O_7 where c differs by 2.5%, resulting in a volume difference of 0.4–2.8%.

Table 8 contains the calculated properties of VO, V_2O_3, VO_2, V_6O_{13}, V_4O_9, V_3O_7 and V_2O_5. The data provided are vanadium valency, oxygen content in the phases, energy of formation E_f, volume, bulk modulus B, elastic constant C_{44} and B/C_{44}. The elastic data are given for (i) uniform compression (single relaxation at equilibrium) and (ii) with full structural relaxation at every volume. C_{44} is used as a measure of the shear modulus and the B/C_{44} ratio may be interpreted as a measure of plasticity [30, 31].

For all calculated phases the energy of formation with respect to the elements is negative. However, for VO E_f with respect to the elements is -1.778 eV/atom and therefore much higher than for the other phases, which are within the range of -2.635 to -2.794 eV/atom. For the ideal, defect-free stoichiometric VO (rock salt structure), as described here, E_f lies clearly above the ground-state convex hull of the energy-composition diagram, suggesting decomposition in the neighbouring, stable phases V and V_2O_3. Defect-stabilized rock salt structured VO_x ($0.8 \leqslant x \leqslant 1.3$) was considered previously [58–60]. A stable stoichiometric phase has been reported with a vacancy concentration of approximately 15% at metal and oxygen sites [58]. DFT-based calculations on the stability of vanadium oxide growing on metal surfaces have been carried out by Kresse *et al* [8]. It was shown that a stoichiometric VO defect structure with a 25% metal and oxygen vacancy concentration is stable with respect to V and V_2O_3. Since these defects are not within the scope of this study, we will omit any further discussion on VO due to its apparent structural instability. For V_4O_9, the energy of formation is -2.766 eV/atom and hence above both $E_f(V_6O_{13}) = -2.794$ and $E_f(V_3O_7) = -2.773$ eV/atom. It therefore lies slightly above the ground-state convex hull of the energy-composition diagram, suggesting decomposition in the neighbouring phases V_6O_{13} and V_3O_7.

In all discussions below, B and C_{44} data for full structural relaxation for every volume are considered. These values are shown in figure 1 as a function of vanadium valency. As the V valency is increased from 3 to 5, B decreases by 61% from 222 to 87 GPa. For V_nO_{2n+1} series phases V_6O_{13} and V_3O_7, B is approximately 160 GPa. However, for V_4O_9 B is 104 GPa. This relatively low value in relaxed mode (ii) and the corresponding energy–volume curve (not shown here) may indicate a possible phase transformation. Also, according to the E_f data, V_4O_9 is unstable with respect to its neighbouring phases V_6O_{13} and V_3O_7. Hence, we will omit further discussion of this phase. Structural prototypes of V_2O_3 and VO_2 are corundum (α-Al_2O_3) and rutile (TiO_2), respectively. For corundum and rutile, the calculated B values are 232 and 213 GPa, differing by 4.5% and 6.2% from the vanadium oxide counterparts, respectively. Experimental data of 246 GPa for corundum [61] and 212 GPa for rutile [62] are consistent with our calculations. As the valency of vanadium is increased from 3 to 5, the C_{44} values decrease by 83% from 153 to 25 GPa. V_2O_3 and VO_2 exhibit, with 153 and 128 GPa, C_{44} values similar to their prototypes, corundum (133 GPa calculated here, 147 GPa experimental [61]) and rutile (127 GPa calculated here, 124 GPa experimental [62]), respectively. However, as the V valency is increased to >4 for V_6O_{13} and V_3O_7, C_{44} significantly decreases to 76 and 63 GPa, respectively, and drops down to 25 GPa for V_2O_5. Thus, these phases constitute easily plastically deformable structures, despite comparatively large bulk moduli. The calculated C_{44} value of -89 GPa for defect-free, stoichiometric VO is negative, suggesting structural instability [63], which is consistent with our discussion above.

The B/C_{44} ratio for the vanadates discussed here (except VO and V_4O_9) are shown in figure 2 as a function of vanadium valency. Experimental values for diamond, known solid lubricants, such as silver and gold [64], as well as

Table 8. Calculated properties of the vanadium oxides VO, V_2O_3, VO_2, V_6O_{13}, V_4O_9, V_3O_7 and V_2O_5. The table presents vanadium valency, oxygen content and energy of formation E_f for each phase, as well as volume per atom V, bulk modulus B, elastic constant C_{44} and B/C_{44} ratio. Elastic data are given for (i) uniform compression and (ii) with full structural relaxations for every volume.

		VO	V_2O_3	VO_2	V_6O_{13}	V_4O_9	V_3O_7	V_2O_5
Valency		2	3	4	4.333	4.5	4.667	5
Oxygen content		0.5	0.6	0.667	0.684	0.692	0.7	0.714
E_f (eV/atom)		−1.778	−2.636	−2.770	−2.794	−2.766	−2.773	−2.733
V (Å^3/atom)		9.169	9.687	9.897	11.545	11.858	11.838	13.051
(i)	B (GPa)	243.6	253.8	248.5	208.1	197.3	202.3	173.5
	C_{44} (GPa)	−88.6	165.2	155.1	74.7	78.6	75.5	40.2
	B/C_{44}		1.54	1.60	2.79	2.51	2.68	4.32
(ii)	B (GPa)	243.6	221.7	226.6	166.7	103.7	158.0	86.6
	C_{44} (GPa)	−88.6	153.3	127.8	75.9	66.3	63.2	25.3
	B/C_{44}		1.45	1.77	2.20	1.57	2.50	3.42

Table 9. Decohesion energies for cleavage of {100} and {200} planes in each independent lattice direction in VO_2 and V_2O_5.

	Structure									
	VO_2				V_2O_5					
Plane	{100}	{200}	{001}	{002}	{100}	{200}	{010}	{020}	{001}	{002}
G (J m^{-2})	4.57		2.15		0.69		1.21		4.06	0.05

calculated values for MAX phase nanolaminates Ti_3SiC_2 [65] and Y_2AlC [66] are included for comparison. As the V valency is increased from 3 to 5, the B/C_{44} ratio increases by a factor of 2.4 from 1.4 to 3.4. V_2O_3 and VO_2 exhibit B/C_{44} ratios of 1.4 and 1.8, respectively. According to the data provided in figure 1, these ratios are similar to those of their prototypes corundum and rutile, which are not included in figure 2. For V_6O_{13} and V_3O_7, B/C_{44} ratios of 2.2 and 2.5, respectively, are larger than solid lubricant silver and Ti_3SiC_2. The largest B/C_{44} ratio is obtained for V_2O_5 with 3.4 approaching the ratio for gold. Due to their large B/C_{44} ratios, these oxides are expected to possess lubricating properties.

In order to identify possible shear planes for VO_2 and V_2O_5, decohesion energies for cleavage G were calculated for {100} and {200} planes in each independent lattice direction (see table 9). These phases are chosen because they exhibit a large difference in B/C_{44}. Due to the VO_2 symmetry, $P4_2/mnm$, cleaving in (100), (200), (010) and (020) planes yields identical results, $G = 4.57$ J m^{-2}, while cleaving in (001) and (002) planes gives 2.15 J m^{-2}. For V_2O_5, $Pmmn$ structure, cleaving in (100) and (200) planes results in 0.69 and 0.70 J m^{-2}, respectively. Within the accuracy of these calculations, the latter two values can be considered identical as expected, due to symmetry. For cleaving in the equivalent (010) and (020) planes, $G = 1.21$ J m^{-2} is obtained. Cleaving V_2O_5 in (001) and (002) planes results in a decohesion energy of 4.06 and 0.05 J m^{-2}, respectively. Obviously, there is a large anisotropy in decohesion energies, especially in the case of V_2O_5, for which the spread is over two orders of magnitude. The decohesion energies calculated here for V_2O_5 are consistent with the surface energy data obtained previously [12]. The lowest decohesion energies in each direction for VO_2 and V_2O_5 are presented in figure 3. For comparison, decohesion energy for the basal plane of MAX phases Ti_2AlC and Cr_2AlC [67] as well as for the (100) and the (110) plane of NiAl [57] are included. V_2O_5 shows an anisotropic behaviour with the value for the V_2O_5(002) plane cleavage being extremely low. It is only 2.8%, 2.0% and 1.6% of the decohesion energies for Ti_2AlC(0001), Cr_2AlC(0001) and NiAl(110), respectively. This very low decohesion energy is comparable with the surface energy of graphite (0.08 J m^{-2}) [54]. Furthermore, these data are consistent with the B/C_{44} ratios presented above. Thus, we expect that

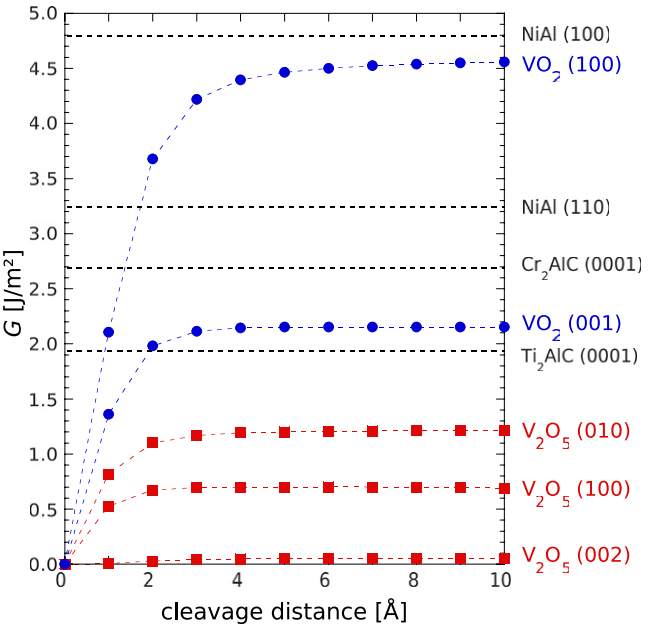

Figure 3. Decohesion energy G as a function of the distance between the cleaved blocks. Circles (blue) present VO_2, squares (red) V_2O_5. MAX phases Ti_2AlC and Cr_2AlC [67], as well as NiAl [57] are included for comparison.

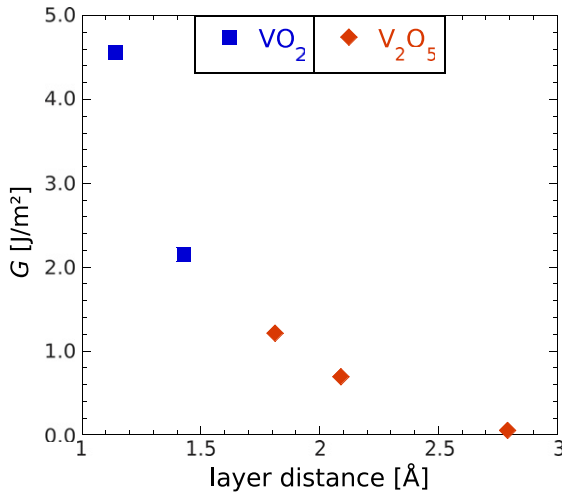

Figure 4. Decohesion energy as a function of the layer distance for the {200} planes of VO_2 (squares/blue) and V_2O_5 (diamonds/red).

this easy cleaving plane enables plastic deformation and is therefore responsible for the vanadium pentoxide's lubricating properties.

These decohesion energies can be related to the (original) distance between the cleaved crystal layers, as shown in figure 4. Short layer distance results in high decohesion energy, as seen for VO_2, where distances of 1.14 and 1.43 Å result in decohesion energies of 4.57 and 2.15 J m^{-2}, respectively. Accordingly, large distance results in low decohesion energy, as can be seen for the V_2O_5(002) plane with a distance of 2.83 Å, resulting in a decohesion energy of 0.05 J m^{-2}. Our data suggest that the bonding distance between the cleaved layers is one of the key factors determining the decohesion energy for the phases studied here.

The elastic properties and decohesion energies of these vanadium oxides may be understood based on the electronic structure. Electron density distribution obtained by the *ab initio* calculations are presented for V_2O_3 and VO_2 in figure 5 and V_6O_{13}, V_3O_7 and V_2O_5 in figure 6. In general, these oxides may be characterized by ionic bonding, due to the charge transfer from vanadium to oxygen. To some extent, there is charge shared between these two elements, giving rise to a smaller covalent contribution. In particular for the V_2O_5 vanadyl bond, covalent character is apparent. It is important to note that these EDDs never exhibit regions without charge (0 eV Å^{-3}), which may indicate that some minor metallic contributions are present. However, striking differences between these phases can be observed. In V_2O_3 and especially in VO_2 (figure 5), there are only very small regions with low electron density between the ions, or rather between the V–O polyhedra. This in turn may imply relatively strong bonding. Ionic structures, such as NaCl, are strongly bonded because of the large charge difference and the short distance between neighbouring atoms. For V_6O_{13}, V_3O_7 and especially V_2O_5 (figure 6), there are very large regions with low electron density. In particular, two distinctive regions within the EDDs can be identified: (i) regions with high electron density and (ii) regions with low electron density. The high electron density

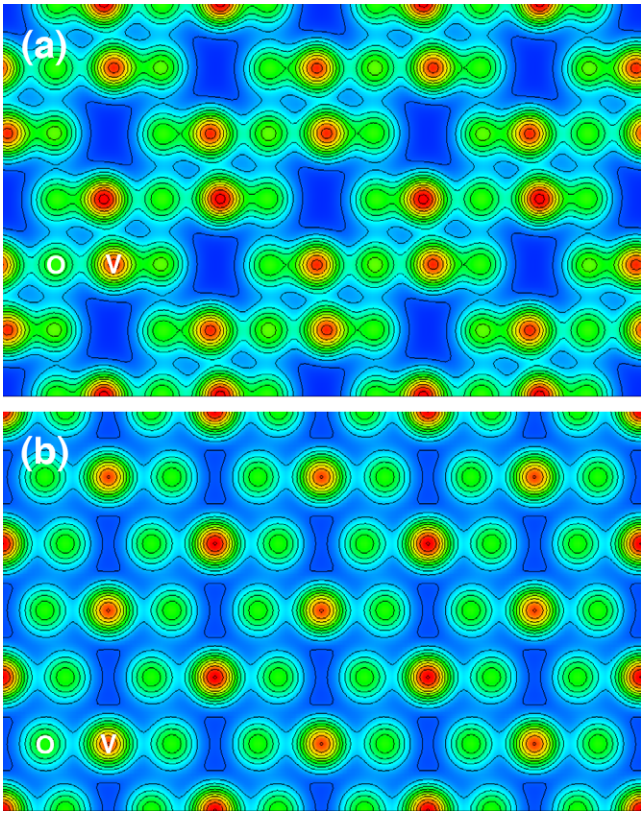

Figure 5. Electron density distribution of (a) V_2O_3 projected along the [100] axis (1 × 2 supercell) and (b) VO_2 projected along the [100] axis (3 × 3 supercell). The EDD increases from 0.0034 to 2.159 and from 0.0047 to 2.141 a.u., respectively. Within this ionic structure, there is a minor contribution from covalent and metallic bond character, since a non-negligible electron density between the ions can be seen. No distinct shear planes are identifiable.

regions may be assigned to V–O polyhedra, separated by the low electron density regions between the V–O polyhedra, or rather between the layers. Thus, only weak ionic bonding between the layers is established. Upon insertion of free electrons, as argued above, the Coulomb potential may be screened so that an exponential term should be added [64]. We suggest that the screened Coulomb potential and the presence of large low electron density regions in V_6O_{13}, V_4O_9, V_3O_7 and V_2O_5 are responsible for low C_{44} values and therefore enable easy plastic deformation.

4. Conclusion

Different vanadium oxide phases ranging from V valency 2 to 5, including VO, V_2O_3, VO_2, V_6O_{13}, V_4O_9, V_3O_7 and V_2O_5, have been investigated in terms of bulk modulus and elastic constant C_{44} using *ab initio* calculations. As the V valency is increased from 3 to 5, C_{44} decreases from 153 to 25 GPa, whereas the bulk modulus values decrease from 222 to 87 GPa. Vanadium(III)- and vanadium(IV) oxide have similar bulk moduli and C_{44} values as their structural prototypes corundum and rutile. The most promising properties in terms of solid lubrication, e.g. for protective coatings in metal cutting applications, are observed for vanadium pentoxide. In this

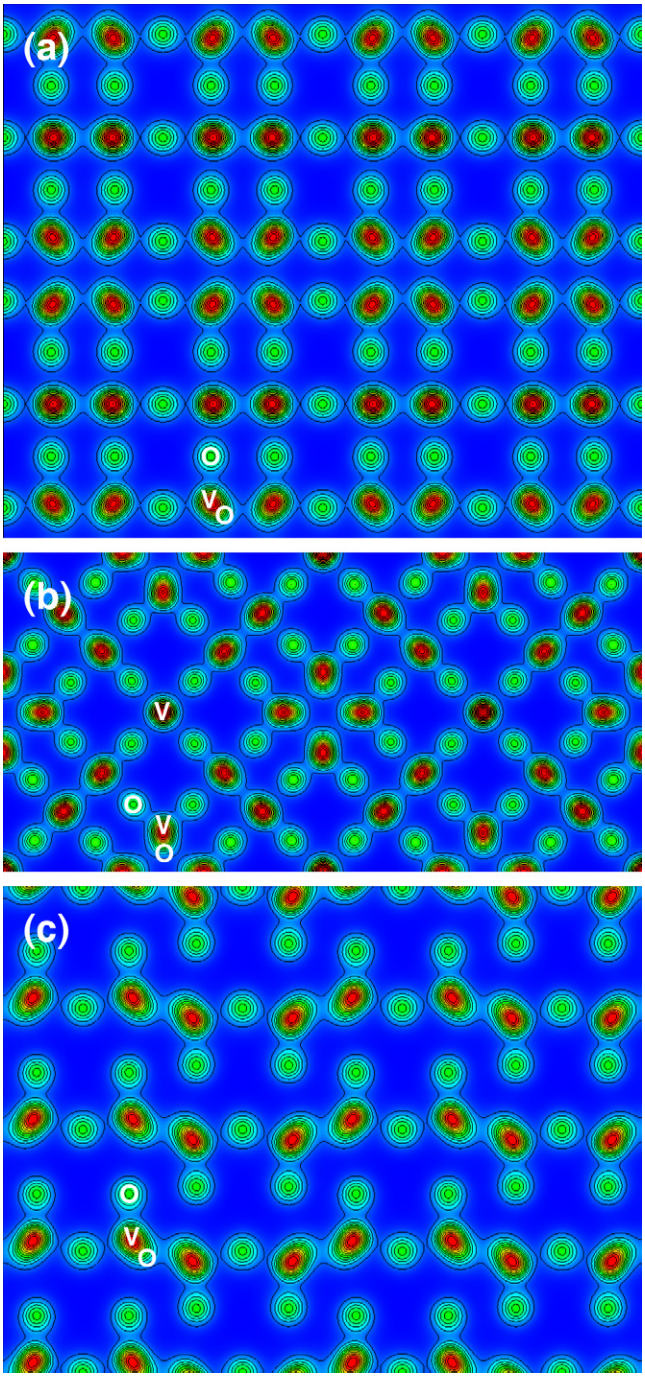

Figure 6. Electron density distribution of (a) V_6O_{13}, projected along the [001] axis (2 × 1 supercell), (b) V_3O_7, projected along the [001] axis (2 × 1 supercell) and (c) V_2O_5 projected along the [010] axis (2 × 4 supercell). The EDD increases from 0.0003 to 2.139, 2.134 and 2.131 a.u., respectively.

phase, vanadium is in its highest oxidation state. When oxidizing vanadium from V_2O_3 to V_2O_5, the V valency induced change in the crystal and bonding structure causes the B/C_{44} ratio to increase from 1.4 to 3.4. This is consistent with calculated decohesion energies of VO_2 and V_2O_5. The lowest decohesion energy for VO_2 is 2.15 J m^{-2}, whereas for V_2O_5 it is 0.05 J m^{-2}, being extremely low in comparison to other cleavage directions in the same structure and that by at least a factor of 10. This very low decohesion energy is similar to the calculated surface energy for graphite (0001) (0.08 J m^{-2}) [54]. The bonding of phases exhibiting high C_{44} values is predominantly ionic with some minor contributions of covalent and metallic character. Due to the screened Coulomb potential between the layers in the phases exhibiting low C_{44} values, such as V_6O_{13}, V_4O_9, V_3O_7 and V_2O_5, the bond strength decreases rapidly as the distance is increased, resulting in weak coupling between the layers which then causes the formation of easily plastically deformable structures.

Acknowledgments

The authors gratefully acknowledge funding from the Federal Ministry of Education and Research of the Federal Republic of Germany and their framework programme 'Materials innovations for industry and society' (Werkstoffinnovationen für Industrie und Gesellschaft—WING), represented by Projektträger Jülich, for project FKZ: 03X3507C.

References

[1] Stringer J 1965 *J. Less-Common Met.* **8** 1–14
[2] Katzke H, Tolédano P and Depmeier W 2003 *Phys. Rev.* B **68** 024109
[3] Fiermans L, Clauws P, Lambrecht W, Vandenbroucke L and Vennik J 1980 *Phys. Status Solidi* a **59** 485–504
[4] Schwingenschlögl U and Eyert V 2004 *Ann. der Phys.* **13** 475–510
[5] Andersson G 1954 *Acta Chem. Scand.* **8** 1599–606
[6] Tilley R J D and Hyde B G 1970 *J. Phys. Chem. Solids* **31** 1613–9
[7] Gellings P J 1985 *Catalysis* vol 7, ed G Webb and G C Bond (London: The Royal Society of Chemistry)
[8] Kresse G, Surnev S, Ramsey M G and Netzer F P 2001 *Surf. Sci.* **492** 329–44
[9] Chakrabarti A, Hermann K, Druzinic R, Witko M, Wagner F and Petersen M 1999 *Phys. Rev.* B **59** 10583–90
[10] Hermann K, Witko M, Druzinic R, Chakrabarti A, Tepper B, Elsner M, Gorschluter A, Kuhlenbeck H and Freund H J 1999 *J. Electron Spectrosc. Relat. Phenom.* **98/99** 245–56
[11] Brázdová V, Ganduglia-Pirovano M V and Sauer J 2004 *Phys. Rev.* B **69** 165420
[12] Ganduglia-Pirovano M V and Sauer J 2004 *Phys. Rev.* B **70** 045422
[13] Morin F J 1959 *Phys. Rev. Lett.* **3** 34–6
[14] Goodenough J B 1971 *Annu. Rev. Mater. Sci.* **1** 101–38
[15] Honig J M and Zandt L L V 1975 *Annu. Rev. Mater. Sci.* **5** 225–78
[16] Zylbersztejn A and Mott N F 1975 *Phys. Rev.* B **11** 4383–95
[17] Shin S, Suga S, Taniguchi M, Fujisawa M, Kanzaki H, Fujimori A, Daimon H, Ueda Y, Kosuge K and Kachi S 1990 *Phys. Rev.* B **41** 4993–5009
[18] Imada M, Fujimori A and Tokura Y 1998 *Rev. Mod. Phys.* **70** 1039–263
[19] Schwingenschlögl U, Eyert V and Eckern U 2003 *Europhys. Lett.* **64** 682–8
[20] Adler D 1968 *Rev. Mod. Phys.* **40** 714–36
[21] Kachi S, Kosuge K and Okinaka H 1973 *J. Solid State Chem.* **6** 258–70
[22] Canfield P C, Thompson J D and Gruner G 1990 *Phys. Rev.* B **41** 4850–3
[23] Kawashima K, Ueda Y, Kosuge K and Kachi S 1974 *J. Cryst. Growth* **26** 321–2

[24] Blum R P, Niehus H, Hucho C, Fortrie R, Ganduglia-Pirovano M V, Sauer J, Shaikhutdinov S and Freund H J 2007 *Phys. Rev. Lett.* **99** 226103
[25] Chakraverty B K, Sienko M J and Bonnerot J 1978 *Phys. Rev.* B **17** 3781–9
[26] Franz R, Neidhardt J, Sartory B, Kaindl R, Tessadri R, Polcik P, Derflinger V and Mitterer C 2006 *Tribol. Lett.* **23** 101–7
[27] Fateh N, Fontalvo G A, Gassner G and Mitterer C 2007 *Tribol. Lett.* **28** 1–7
[28] Fateh N, Fontalvo G A and Mitterer C 2008 *Tribol. Lett.* **30** 21–6
[29] Mayrhofer P H, Hovsepian P E, Mitterer C and Münz W D 2004 *Surf. Coat. Technol.* **177/178** 341–7
[30] Pugh S F 1954 *Phil. Mag.* **45** 823–43
[31] Vitos L, Korzhavyi P A and Johansson B 2003 *Nat. Mater.* **2** 25–8
[32] Hartmann H and Mässing W 1951 *Z. Anorg. Allg. Chem.* **266** 98–104
[33] Newnham R E and de Haan Y M 1962 *Z. Kristallogr.* **117** 235–7
[34] Westman S 1961 *Acta Chem. Scand.* **15** 217
[35] Ohno T, Nakamura Y and Nagakura S 1985 *J. Solid State Chem.* **56** 318–24
[36] Wilhelmi K A and Waltersson K 1970 *Acta Chem. Scand.* **24** 3409–11
[37] Darriet J and Galy J 1972 *J. Solid State Chem.* **4** 357–61
[38] Enjalbert R and Galy J 1986 *Acta Crystallogr.* C **42** 1467–9
[39] Hohenberg P and Kohn W 1964 *Phys. Rev.* **136** B864–71
[40] Kresse G and Joubert D 1999 *Phys. Rev.* B **59** 1758–75
[41] Perdew J P and Wang Y 1992 *Phys. Rev.* B **45** 13244–9
[42] Blöchl P E 1994 *Phys. Rev.* B **50** 17953–79
[43] Monkhorst H J and Pack J D 1976 *Phys. Rev.* B **13** 5188–92
[44] Neuburger M C 1936 *Z. Kristallogr.* **93** 314–5
[45] Sutton L E (ed) 1965 *Table of Interatomic Distances and Configuration in Molecules and Ions, Supplement 1956–1959* Special Publication No. 18 (London: The Chemical Society)
[46] Birch F 1978 *J. Geophys. Res.* **83** 1257–68
[47] Mehl M J, Osburn J E, Papaconstantopoulos D A and Klein B M 1990 *Phys. Rev.* B **41** 10311–23
[48] Mehl M J, Klein B M and Papaconstantopoulos D A 1994 *Intermetallic Compounds: Principles and Applications* ed J H Westbrook and R L Fleischer (London: Wiley)
[49] Ravindran P, Fast L, Korzhavyi P A, Johansson B, Wills J and Eriksson O 1998 *J. Appl. Phys.* **84** 4891–904
[50] Fast L, Wills J M, Johansson B and Eriksson O 1995 *Phys. Rev.* B **51** 17431–8
[51] Snyders R, Music D, Sigumonrong D, Schelnberger B, Jensen J and Schneider J M 2007 *Appl. Phys. Lett.* **90** 193902
[52] Music D, Sun Z and Schneider J M 2006 *Solid State Commun.* **137** 306–9
[53] Albe K 1997 *Phys. Rev.* B **55** 6203–10
[54] Ooi N, Rairkar A and Adams J B 2006 *Carbon* **44** 231–42
[55] Momma K and Izumi F 2008 *J. Appl. Crystallogr.* **41** 653–8
[56] Fu C L 1990 *J. Mater. Res.* **5** 971–9
[57] Lazar P and Podloucky R 2006 *Phys. Rev.* B **73** 104114
[58] Banus M D, Reed T B and Strauss A J 1972 *Phys. Rev.* B **5** 2775–84
[59] Watanabe D, Andersson B, Gjønnes J and Terasaki O 1974 *Acta Crystallogr.* A **30** 772–6
[60] Morinaga M and Cohen J B 1976 *Acta Crystallogr.* A **32** 387–95
[61] Gieske J H and Barsch G R 1968 *Phys. Status Solidi* **29** 121–31
[62] Isaak D G, Carnes J D, Anderson O L, Cynn H and Hake E 1998 *Phys. Chem. Miner.* **26** 31–43
[63] Wallace D C 1972 *Thermodynamics of Crystals* (New York: Wiley)
[64] Kittel C 1996 *Introduction to Solid State Physics* 7th edn (New York: Wiley)
[65] Holm B, Ahuja R and Johansson B 2001 *Appl. Phys. Lett.* **79** 1450
[66] Music D, Sun Z, Voevodin A A and Schneider J M 2006 *Solid State Commun.* **139** 139–43
[67] Music D, Houben A, Dronskowski R and Schneider J M 2007 *Phys. Rev.* B **75** 174102